CrossMark

Thermal analyses of yttrium-doped barium zirconate with phosphor pentoxide, boron oxide and zinc oxide addition

R. Muccillo[1] · E. N. S. Muccillo[1] · T. F. Andrade[1] · O. R. Oliveira[1]

Abstract Yttrium-doped barium zirconate (BZY), one of the protonic conductors considered to be used as solid electrolyte in solid oxide fuel cells (SOFC) operating at temperatures lower than the one found in conventional oxide-ion SOFCs, still presents some challenges to reach high density and high electrical conductivity: the difficulty to sinter at temperatures well below its melting point and the blocking of the conducting species at the grain boundaries. We describe an experimental sequence to prepare powders and to obtain highly dense BZY ceramic pellets with enhanced electrical conductivity, using either phosphor pentoxide (P_2O_5), boron oxide (B_2O_3) or zinc oxide (ZnO) as sintering aid. The reactions leading to sintering ceramic pellets with densities higher than 94% of the theoretical density and improved electrical performance are monitored by thermal analyses. BZY with the addition of 5 mass% P_2O_5 or 2 mass% ZnO shows a tenfold enhancement of the electrical conductivity.

Keywords Thermo-gravimetry · Thermo-dilatometry · Barium zirconate · Liquid-phase sintering

Introduction

Ceramic proton conductors have been proposed as potential materials to be used in many diverse applications in several industrial processes, mainly in hydrogen separation membranes, hydrogen sensors for process control and safety monitoring, and also as solid electrolytes in solid oxide fuel–electrolysis cells (SOF-EC) for alternative production of electrical energy from chemical energy [1–7]. Actual technological devices use cubic yttrium-stabilized zirconia (YSZ) as the best solid electrolyte for application in SOFC devices [8] operating at relatively high temperatures (900–1000 °C). Lowering that operation temperature requires solid electrolytes with enhanced electrical conductivity. Yttrium-doped barium zirconate (BZY) ceramic protonic conductor has been proposed as candidate for SOFCs operating at temperatures lower than those used in SOFC devices with YSZ as solid electrolyte [9–13]. Even though its proton conductivity is higher than the oxide-ion conductivity of YSZ, high sintering temperature to obtain high density and blocking of charge carriers at the grain boundaries are the main problems to be solved. Usually very high temperatures are required to produce dense electrolytes [14–16]. A recent review points out to the advantages of nanosized perovskites over their bulk forms, leading to reduced grain boundary resistivity [17]. The importance of using clean environment to process these nanosized perovskites was recently reported [18]. Besides those problems, after finding a way to produce dense pellets with high proton conductivity, keeping the required stoichiometry is a challenge because barium loss upon heating should be avoided [19]. There are many reports on low-temperature sintering of these compounds either by the chemical synthesis of sinter-active powders by the use of sintering aids or by applying special sintering techniques [20–32]. We report here a series of experiments on BZY compounds, synthesized by the low-cost mixture of oxides technique, and sintered using phosphor pentoxide, a powerful dehydrating agent that melts at 340 °C and sublimes at 360 °C, as sintering aid. The main idea for

✉ R. Muccillo
muccillo@usp.br

1 Center of Science and Technology of Materials, Energy and Nuclear Research Institute (CCTM-IPEN), Travessa R 400, Cidade Universitária, São Paulo, SP 05508-170, Brazil

Springer

using P_2O_5 was to withdraw water molecules attached to the barium zirconate ceramic particles before sintering, which might be responsible for the formation of hard particle agglomerates [18, 33], which impedes densification. The increase in the shrinkage level promoted by adding phosphor pentoxide was impressive. The enhancement of the densification of pure barium zirconate upon phosphor pentoxide addition has been reported [34]. Here is reported the densification, the shrinkage behavior and the electrical properties of BZY with the addition of P_2O_5. The blocking of protons at the intergranular regions, ascribed to space charge at the grain boundaries [35], is probably inhibited by the hydrating reaction of phosphor pentoxide with chemical species at the grain boundary region. Looking for low-temperature sintering and improvement on the protonic conductivity, additional results are here reported on the use of B_2O_3, which might act in a liquid-phase sintering mechanism (its melting point is only 450 °C) and ZnO, already reported as sintering aid to BZY [36–39]. The main effect of 4 mol% ZnO addition was to lower the sintering temperature from 1700 to 1300 °C, probably by volatilization of the eutectic BaO.ZnO at that temperature and to improve densification up to 98.5% of the theoretical density. B_2O_3 has been used as sintering aid in polycrystalline ionic conductors [40, 41] and was found to destabilize (cubic to monoclinic) YSZ and 10Sc1CeSZ (ZrO_2:10 mol% Sc_2O_3–1 mol% CeO_2) [42]. Thermogravimetric and differential thermal analyses, along with collecting mass spectrometry data, were performed in BCY compounds without sintering aids looking for conversion of barium cerate to barium carbonate and barium hydroxide [43]. There is no report on the use of B_2O_3 as sintering aid to BZY protonic conductors. The main purpose of this report is to carry out detailed analyses by thermo-analytical techniques of the use of three sintering aids envisaging the production of BZY ceramic pellets dense and with improved electrical properties.

Experimental

$BaZr_{0.8}Y_{0.2}O_{3-\delta}$ compounds were synthesized by solid-state reaction of stoichiometric amounts of BaO, ZrO_2 and Y_2O_3 (all from Alfa Aesar, 99.9%) following the procedure: (1) homogenizing 10 g of the mixture in an agate mortar, (2) calcining in air at 1250 °C for 1 h, (3) homogenizing again, (4) grinding the mixture in an attritor mill with 60 mL of Tosoh Y-TZP (ZrO_2:3 mol% Y_2O_3) 2-mm-diameter grinding medium and 30 mL ethanol for 25 min at 500 rpm, (5) collecting the powder suspension (finer particles) with a fine sieve and (6) drying that suspension at 100 °C overnight. These powders are referred as "as prepared". To improve densification, the powders were

uniaxially pressed at 100 MPa, sintered at 1500 °C for 4 h, crushed and submitted again to attrition milling. This procedure was repeated twice to ensure homogenization and single crystallographic phase. These powders are referred as "attrition-milled powders". The distribution of particle size was evaluated at room temperature with 1 g of powder in a solution of water and sodium pyrophosphate ultrasonically dispersed (Vibra-Cell Sonics & Materials, 5 min) in a granulometer Cilas 1064.

P_2O_5, ZnO and B_2O_3 (all from Alfa Aesar) additions in the 1–5 mass% range were carried out according to the following procedure: (1) mixing the attrition-milled BZY powders with the calculated stoichiometric amounts of P_2O_5, ZnO or B_2O_3 with 30 mL acetone, (2) mixing and drying the mixture on a hot plate at 100 °C, (3) uniaxially and isostatically pressing approximately 600 mg at 100 and 200 MPa, respectively, (4) inserting in a furnace kept at 100 °C and (5) sintering at 1550 °C for 4 h with a 2 °C min^{-1} heating rate and 10 °C min^{-1} cooling rate in a Zircar furnace.

The evolution of the reaction of $BaZr_{0.8}Y_{0.2}O_{3-\delta}$ with the additives was monitored by thermo-gravimetric (TG) and differential thermal (DTA) analyses in a STA 409E Netzsch equipment with a flow of 5 L min^{-1} synthetic air, α-alumina as reference and 10 °C min^{-1} heating and cooling rates. The collected data were processed with the Netzsch Proteus® software for evaluation of peak temperature and area, mass loss, besides smoothing noisy raw data.

The thermo-dilatometric analyses were carried out in an 1161 Anter vertical dilatometer in the RT-1500–200 °C range in air with 10 °C min^{-1} heating rate. Typical samples were uniaxially (10 MPa) and isostatic (30 MPa) pressed cylindrical pellets with dimensions 5 mm diameter and 5 mm thickness.

Geometric and Archimedes apparent densities were evaluated, the latter by using kerosene as liquid medium [44] due to the hygroscopic nature of BZY.

The cubic perovskite phase was evaluated by X-ray diffraction in a Bruker-AXS D8 Advance diffractometer with θ–2θ Bragg–Brentano configuration with CuKα radiation with Ni filter, 40 kV–40 mA power, in the 10°–90° 2θ range, 0.05° step size and 5 s counting time per step.

Impedance spectroscopy measurements were taken in a two-electrode cell at selected temperatures in the 400–700 °C range using a Hewlett Packard 4192A Impedance Analyzer connected to a model 362 Hewlett Packard Controller, in the f = 5 Hz–13 MHz frequency range in sintered cylindrical pellets with parallel surfaces coated with silver electrodes. An Inconel 600 sample chamber holding 3 specimens with platinum leads and a K-type thermocouple was used inside a programmable furnace. A special software was used to collect and analyze the

$[-\mathrm{Im}\, Z(f) \times \mathrm{Re}\, Z(f)]$ data [45], where $\mathrm{Im}\, Z$ and $\mathrm{Re}\, Z$ are the imaginary and the real components, respectively, of the impedance, Eq. 1 [46]. The component values were normalized according to the geometrical factor (sectional area-to-thickness ratio) of the sintered pellets.

$$Z(f) = \mathrm{Re}\, Z(f) + i\,\mathrm{Im}\, Z(f) \qquad (1)$$

SEM analyses were performed in a Inspect F50 FEI scanning electron microscope.

Results and discussion

Synthesis of $BaZr_{0.8}Y_{0.2}O_{3-\delta}$

Figure 1 shows the particle size distribution of $BaZr_{0.92}Y_{0.08}O_{3-\delta}$ powders prepared by solid-state reaction and the effect of attrition milling.

The distribution of the as-prepared powders (Fig. 1a) is bimodal, centered at 10.5 and 80 µm. After milling in the
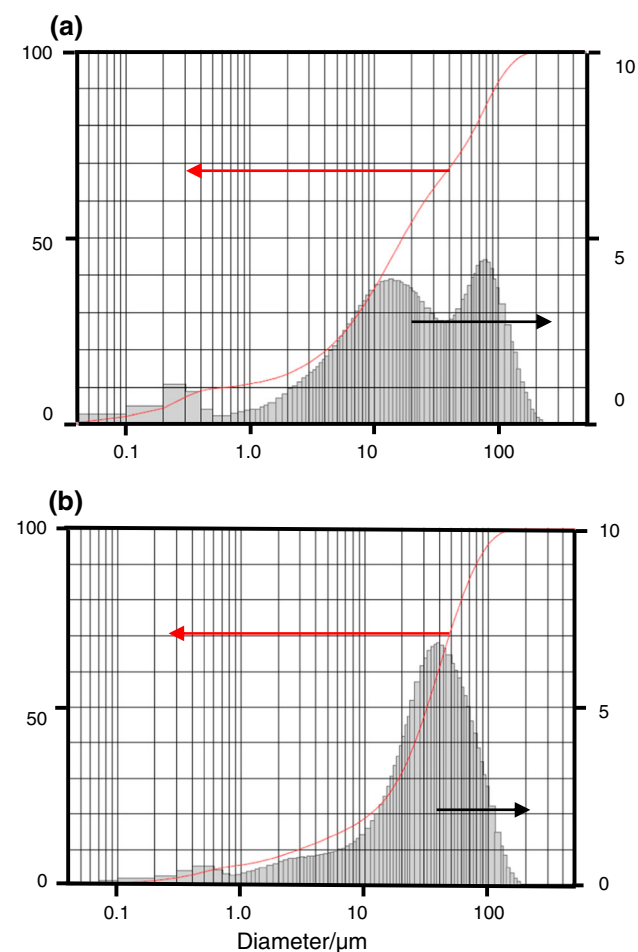
attritor, the distribution (Fig. 1b) approaches to mono-modal centered at ~ 38 µm.

The X-ray diffraction patterns of $BaZr_{0.8}Y_{0.2}O_{3-\delta}$ compounds, prepared by solid-state reaction of $BaCO_3$, ZrO_2 and Y_2O_3, are shown in Fig. 2. Data were collected after the first, the second and the third sintering procedures at 1500 °C for 4 h with intermediate grinding. The triple procedure was performed to assure a high homogeneity of the powder as the X-ray penetration into the specimen under X-ray diffraction analysis is lower than the powder average particle size.

All patterns show the perovskite cubic phase, depicted at the bottom in the same figure, with the nine main reflections indicated by the Miller indexes (JCPDS file #6-399) at the top of the figure.

Figure 3 shows the results of the TG and DTA of the stoichiometric mixture of barium, zirconium and yttrium oxides. The total mass loss is approximately 17.4% in three temperature ranges: from room temperature to approximately 200 °C, due to removal of adsorbed water and to the decomposition of barium hydroxide originated from the water adsorption after handling at room temperature the precursor barium oxide. The endothermic peak at approximately 130 °C is due to that decomposition. The exothermic peak at approximately 370 °C is probable due to dehydration of the compound, as reported after high-temperature X-ray diffraction and thermo-mechanical experiments on BZY [47]. The second mass loss in the 600–800 °C range is due to the decomposition of residual barium carbonate, produced by the exposition of barium oxide to ambient carbon dioxide [47, 48]. The third mass loss in the 1000–1300 °C range is assigned to barium oxide evaporation [Alfa Aesar 2010 catalogue]. These results


Fig. 1 Distribution of particle size of $BaZr_{0.92}Y_{0.08}O_{3-\delta}$ prepared by the mixing of oxides technique: **a** as synthesized, **b** after attrition milling
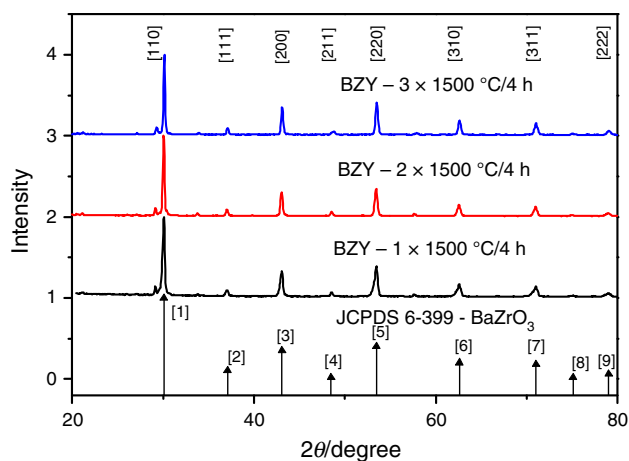
Fig. 2 X-ray diffraction patterns of $BaZr_{0.8}Y_{0.2}O_{3-\delta}$ ceramic powders prepared by mixing and heat treating a mixture of zirconium, yttrium and barium oxides. Effect of sequential milling–sintering procedure. Miller indices on *top*
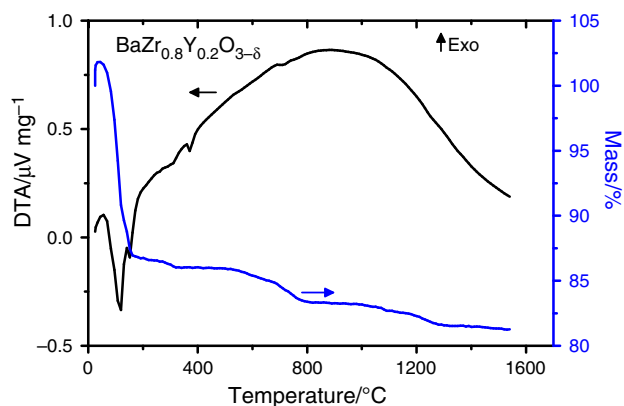
Fig. 3 Thermo-gravimetric (TG) and differential thermal analysis (DTA) curves of the oxide powder mixture to prepare the $BaZr_{0.8}Y_{0.2}O_{3-\delta}$ compound

show that the temperature to complete the reaction of formation of the $BaZr_{0.8}Y_{0.2}O_{3-\delta}$ compound is approximately 1300 °C.

Figure 4 shows the X-ray diffraction pattern of $BaZr_{0.92}Y_{0.2}O_{3-\delta}$ surface of pellets sintered at 1550 °C for 4 h using BZY powders processed three times at 1500 °C for 4 h (Fig. 2) and, for comparison purposes, the JCPDS 6-399 file. The sintered pellets have the perovskite cubic crystalline structure.
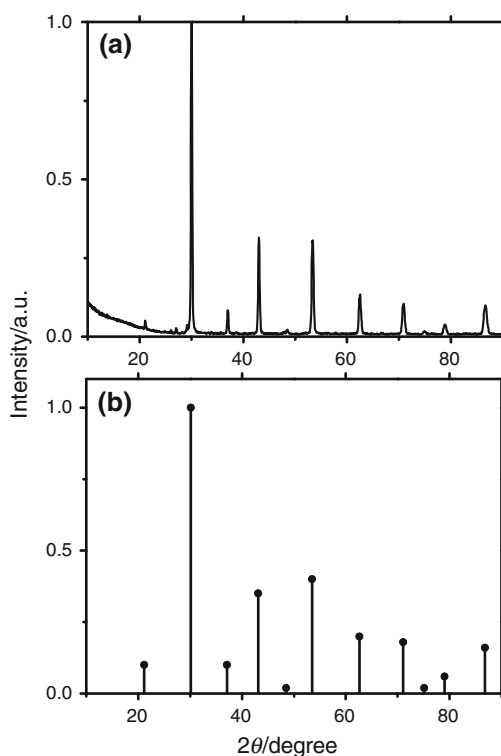
Fig. 4 X-ray diffraction patterns of sintered $BaZr_{0.92}Y_{0.08}O_{3-\delta}$ pellet surface (**a**); data from JCPDS 6-399 file (**b**)
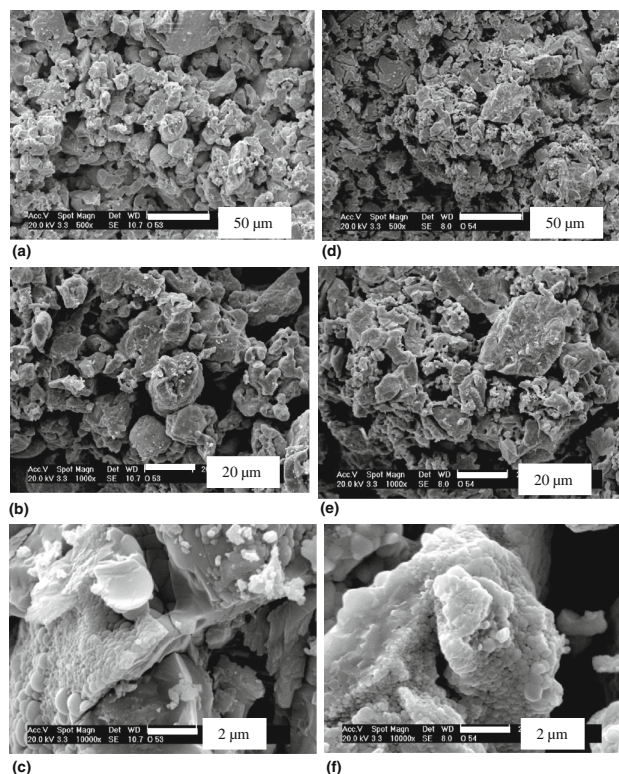
Fig. 5 SEM micrographs of the fracture surfaces of $BaZr_{0.92}Y_{0.08}O_{3-\delta}$ pellets sintered using powders synthesized without (**a–c**) and with (**d–f**) attrition milling
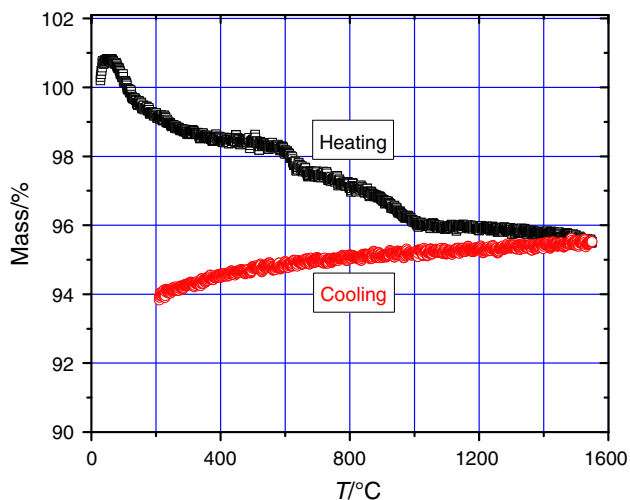
Figure 5 shows the images of the fracture surfaces of $BaZr_{0.8}Y_{0.2}O_{3-\delta}$ pellets sintered at 1550 °C for 4 h. Figure 5a–c corresponds to pellets prepared with powders manually mixed, pressed and sintered. The other three micrographs (Fig. 5d–f) correspond to pellets prepared with powders after comminuting by attrition milling.

All images show that the pellets have high porosity, which is a characteristic of these compounds when sintered at that temperature, without liquid-phase sintering aids. There are differences in shape and size of the particles, depending on the preparation route. Powders processed in the attritor show less rounded shapes, reduction in open porosity, but larger agglomerates probably due to an increase in temperature during the high-energy milling process, known to produce hard agglomerates.

Sintering aid: P_2O_5

The reaction of BZY with P_2O_5 was monitored by TG analysis of 0.95 BZY + 0.05 P_2O_5. The result is shown in Fig. 6.

The total mass loss reaction is completed at approximately 1000 °C. The loss up to 400 °C is due to release of adsorbed and structural water [47], at 340–360 °C due to
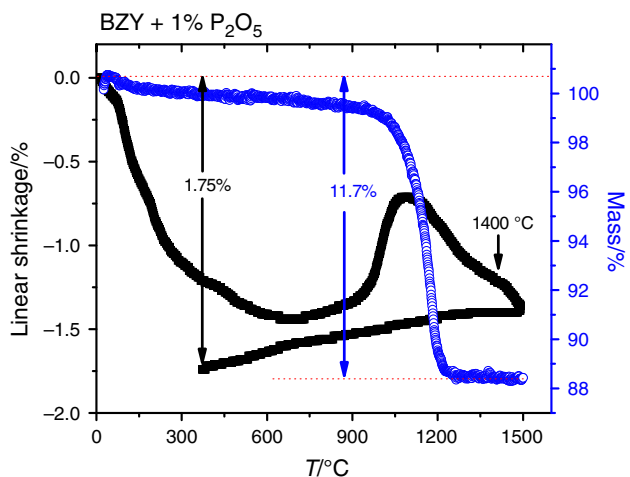
Fig. 6 Thermo-gravimetric (TG) curves of $BaZr_{0.8}Y_{0.2}O_{3-\delta}$ + 5% P_2O_5

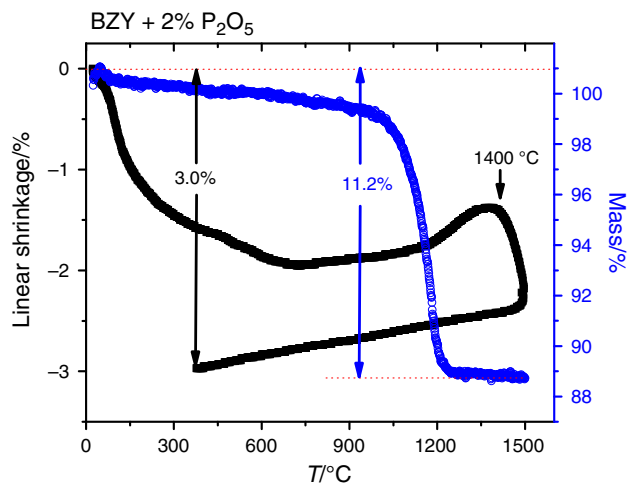**Fig. 8** Thermo-dilatometric curve of green pellets and mass loss of powders of $BaZr_{0.8}Y_{0.2}O_{3-\delta}$ + 2 mass% P_2O_5

melting and evaporation of P_2O_5 and afterward to the decomposition of remaining barium carbonate resulting from the synthesis of BZY in non-controlled atmosphere (in air). The total mass loss is approximately 5%, part due to water and the rest to P_2O_5 added to BZY. A further 1% is lost upon cooling down to 200 °C due to reaction of barium with CO_2 and O_2 of the atmosphere.

The next three figures (Figs. 7–9) show the monitoring of the shrinkage level of pressed pellets of BZY with 1, 2 and 5 mass% P_2O_5, respectively. The mass loss evaluated by TG is also shown.
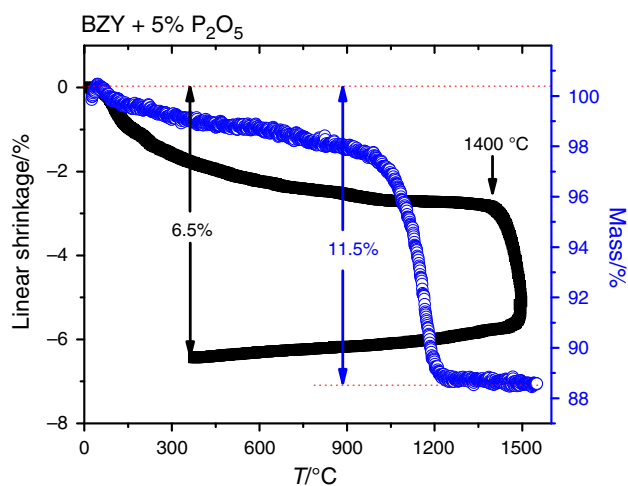
In all these figures, the mass loss corresponds to volatilization of P_2O_5. Moreover, carbon oxide and water, known to easily be adsorbed at BZY compounds, are also thermally removed. Interesting are the results on the shrinking upon heating. Shrinkage as well as expansion
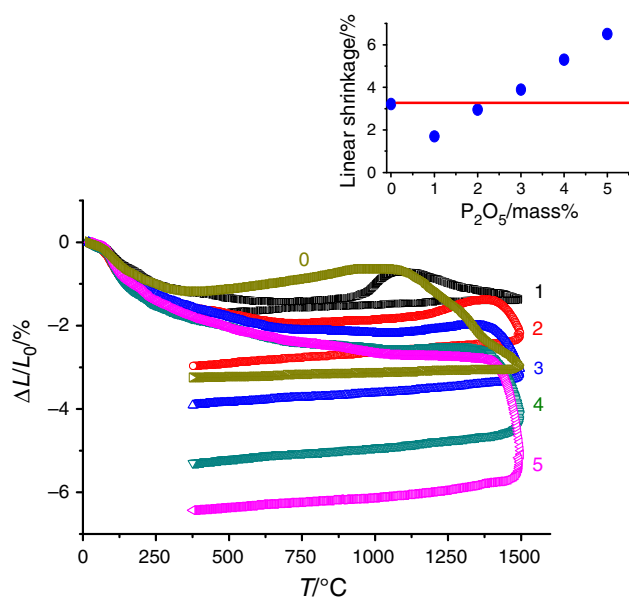

Fig. 9 Thermo-dilatometric curve of green pellets and mass loss of powders of $BaZr_{0.8}Y_{0.2}O_{3-\delta}$ + 5 mass% P_2O_5

occurs, depending on the amount of phosphor pentoxide addition. The final attained shrinkage level is 1.75, 3.0 and 6.5% for 1, 2 and 5 mass% P_2O_5 addition, respectively. The enhancement of sintering with that additive is probably due to liquid-phase sintering: Melting of P_2O_5 might wet the BZY particles which by subsequent heating might be removed from the specimens causing pore elimination by capillarity.

Figure 10 shows results of thermo-dilatometric measurements on $BaZr_{0.8}Y_{0.2}O_{3-\delta}$ with and without the addition of P_2O_5. The dependence of the degree of final shrinkage on the P_2O_5 content is also shown (inset). Apparently the larger is the amount of the sintering aid, the higher is the shrinkage effect for contents larger than ~ 2.5 mass%.

Fig. 7 Thermo-dilatometric curve of green pellets and mass loss of powders of $BaZr_{0.8}Y_{0.2}O_{3-\delta}$ + 1 mass% P_2O_5
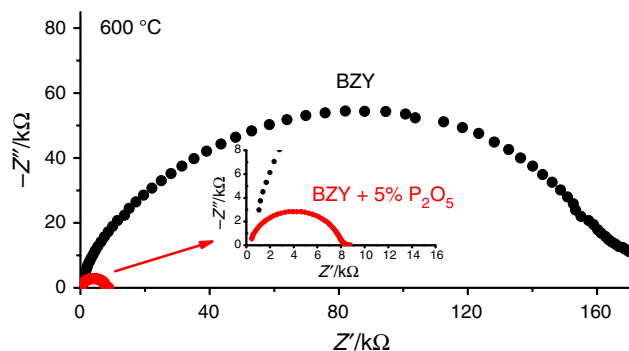
Fig. 10 Thermo-dilatometric curves in the room temperature—1500 °C of green pellets of $BaZr_{0.8}Y_{0.2}O_{3-\delta}$ + x mass% P_2O_5, $x = 0, 1, 2, 3, 4$ and 5. *Inset* final shrinkage level as a function of the P_2O_5 content

Figure 11 shows impedance spectroscopy diagrams measured at 600 °C of $BaZr_{0.8}Y_{0.2}O_{3-\delta}$ sintered without and with 5 mass% P_2O_5. The decrease in the electrical resistance is remarkable, showing a full suppression of the grain boundary blocking of charge carriers, an indication that melted P_2O_5 reacts at the space charge layer, removing the species responsible for the blocking of protons at these interfaces. The total resistivity decreases from 345 to 31.6 kΩ cm.

Sintering aid: B_2O_3

Figure 12 shows the results of the X-ray diffraction analysis of $BaZr_{0.8}Y_{0.2}O_{3-\delta}$ without and with the addition of 1,
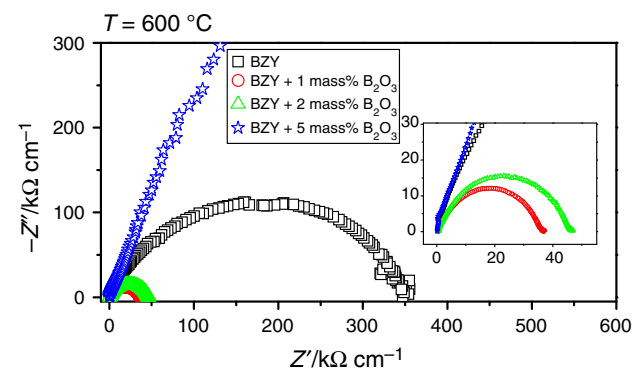
2 and 5 mass% B_2O_3 along with the main reflection lines of $BaZrO_3$, JCPDS 6-399 file.

The diffraction patterns show the BZY pellets sintered with B_2O_3 addition present cubic perovskite single phase, characteristic of $BaZrO_3$ compounds, similar to the specimens sintered with P_2O_5 addition.

Figure 13 shows the impedance diagrams measured at 600 °C of $BaZr_{0.8}Y_{0.2}O_{3-\delta}$ pellets sintered at 1500 °C without and with the addition of B_2O_3. The diagrams consist of one semicircle due to contribution to the total electrical resistivity, including bulk and interfaces, mainly grain boundaries. The enhancement of the electrical conductivity is nearly a tenfold increase: 2.9 μS cm^{-1} (pure BZY) to 27 μS cm^{-1} (1 mass% B_2O_3 addition). Increasing the amount of sintering aid (2 and 5 mass%) did not improve the electrical conductivity, probably by formation of a thick intergranular amorphous phase [34], difficult to analyze due to the low Z value of the boron element.
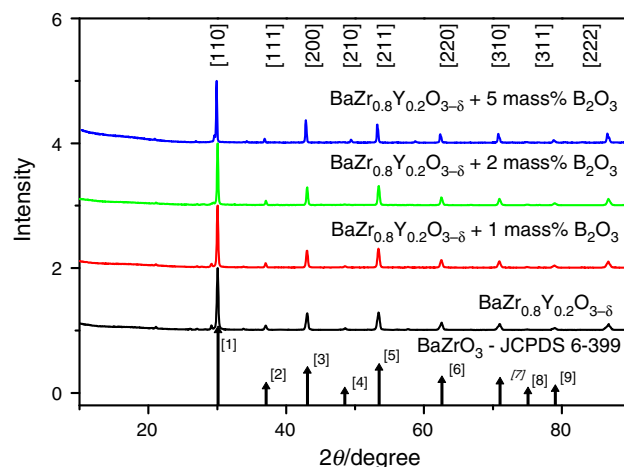
Fig. 12 X-ray diffraction patterns of sintered $BaZr_{0.8}Y_{0.2}O_{3-\delta}$ pellets without and with B_2O_3 addition (1, 2 and 5 mass%). *Bottom lines* refer to $BaZrO_3$ JCPDS 6-399 file. Miller indices on *top*

Fig. 11 Impedance spectroscopy diagrams of $BaZr_{0.8}Y_{0.2}O_{3-\delta}$ and $BaZr_{0.8}Y_{0.2}O_{3-\delta}$ + 5% P_2O_5 sintered pellets. Temperature of measurement: 600 °C. *Inset* high-frequency region

Fig. 13 Impedance spectroscopy diagrams measured at 600 °C of $BaZr_{0.8}Y_{0.2}O_{3-\delta}$ solid electrolytes sintered at 1500 °C without and with B_2O_3 additions. *Inset* detail of the high-frequency region
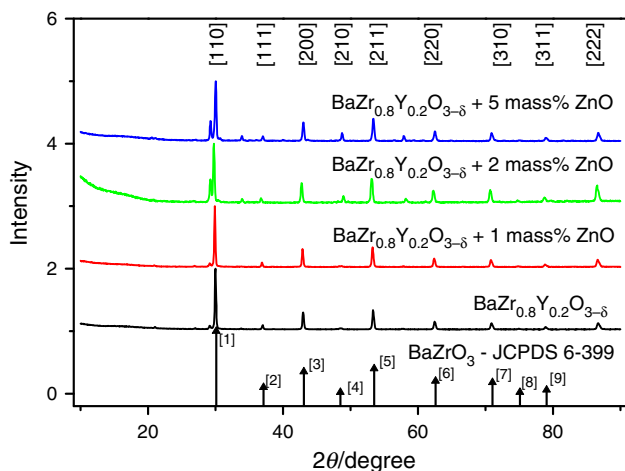
Fig. 14 X-ray diffraction patterns of $BaZr_{0.8}Y_{0.2}O_{3-\delta}$ pellets sintered without and with the addition of 1, 2 and 5 mass% ZnO and without ZnO. *Bottom lines* refer to $BaZrO_3$ JCPDS 6-399 file. Miller indices on *top*

Sintering aid: ZnO

Figure 14 shows the results of the X-ray diffraction analysis of sintered (1500 °C for 4 h) $BaZr_{0.8}Y_{0.2}O_{3-\delta}$ pellets prepared with powders without and with ZnO addition (1, 2 and 5 mass%). The reflection lines of pure $BaZrO_3$ are also depicted, according to the JCPDS 6-399 file.

Similar to the results on $BaZr_{0.8}Y_{0.2}O_{3-\delta}$ pure and sintered with P_2O_5 or B_2O_3 addition, here also the structure is the perovskite cubic.

Figure 15 shows the impedance diagrams measured at 600 °C of $BaZr_{0.8}Y_{0.2}O_{3-\delta}$ pellets sintered at 1500 °C with and without the addition of ZnO.

It is apparent the beneficial effect of the addition of ZnO to the decrease in the intergranular resistivity. At 600 °C, the resistivity decreases 50% with only 1 mass% ZnO added to the yttrium-doped barium zirconate. 2 mass% seems to be
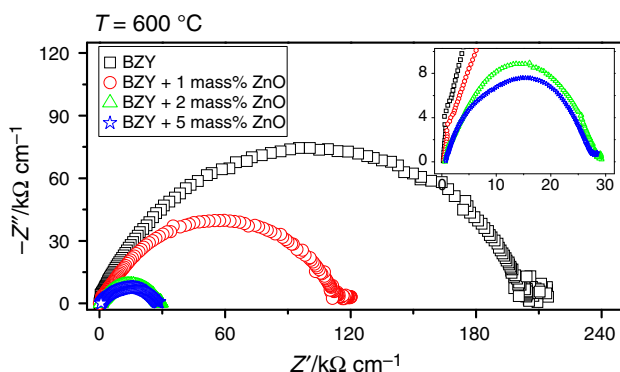
Table 1 Values of electrical resistivity and apparent density of $BaZr_{0.8}Y_{0.2}O_{3-\delta}$ sintered at 1500 °C for 4 h without and with additives

Compound	Electrical resistivity @600 °C/kΩ cm	Density/%T.D.
BZY	345.0	86.1
BZY + 5 mass% P_2O_5	31.6	95.0
BZY + 1 mass% B_2O_3	34.0	86.5
BZY + 2 mass% ZnO	30.0	94.8

T.D.: theoretical density—6.21 g cm^{-3}, evaluated using X-ray diffraction data

the optimum amount of ZnO to be added for improvement of the electrical conductivity. The electrical resistivity at 600 °C drops from 345 kΩ cm for a BZY without to 30 kΩ cm to BZY with 2 mass% ZnO addition. Table 1 shows the values of total (bulk plus interfaces, mainly grain boundaries) electrical resistivity measured at 600 °C and the apparent density of the various sintered compounds.

These values show that the three sintered aids are effective on reducing the total electrical resistivity, but only P_2O_5 and ZnO promote densification higher than 94% of the theoretical density. Moreover, P_2O_5 is believed to act as a catalytic agent, in the sense that it accelerates the densification without taking part in the obtained solid electrolyte (BZY).

Conclusions

Thermo-gravimetry (TG), differential thermal analysis (DTA) and thermo-dilatometry on yttrium-doped barium zirconate (BZY) compounds mixed to phosphor pentoxide (P_2O_5), boron oxide (B_2O_3) and zinc oxide (ZnO) allowed for explaining their densification and the enhancement in the electrical conductivity. The procedures with the results reported here namely the attainment of high density and the enhancement of the electric conductivity might be extended to other novel protonic conductors.

Fig. 15 Impedance spectroscopy diagrams measured at 600 °C of $BaZr_{0.8}Y_{0.2}O_{3-\delta}$ solid electrolytes sintered without and with ZnO additions 600 °C. *Inset* detail of the high-frequency region

References

1. Iwahara H, Asakura Y, Katahira K, Tanaka M. Prospect of hydrogen technology using proton-conducting ceramics. Solid State Ion. 2004;168:299–310.
2. Phair JW, Badwal SPS. Review of proton conductors for hydrogen separation. Ionics. 2006;12:103–15. doi:10.1007/s11581-006-0016-4.

3. Fabbri E, Bi L, Pergolesi D, Traversa E. Towards the next generation of solid oxide fuel cells operating below 600°C with chemically stable proton-conducting electrolytes. Adv Mater. 2012;24:195–208. doi:10.1002/adma.201103102.

4. Park K-Y, Seo Y, Kim KB, Song S-J, Park B, Park J-Y. Enhanced proton conductivity of yttrium-doped barium zirconate with sinterability in protonic ceramic fuel cells. J Alloys Cmpd. 2015;639:435–44. doi:10.1016/j.jallcom.2015.03.168.

5. Duan C, Tong J, Shang M, Nikodemski S, Sanders M, Ricote S, Almansoori A, O'Hayre R. Readily processed protonic ceramic fuel cells with high performance at low temperatures. Science. 2015;349:1321–6.

6. Bi L, Shafi SP, Traversa E. Y-doped BaZrO3 as a chemically stable electrolyte for proton-conducting solid oxide electrolysis cells (SOECs). J Mater Chem A. 2015;3:5815–9. doi:10.1039/c4ta07202b.

7. Gawel R, Przybylski K, Viviane M. Resistance of composite materials based on $BaCeO_3$ against the corrosive effects of carbon dioxide and water vapour at intermediate fuel cell operating temperatures. J Therm Anal Calorim. 2014;116:895–903.

8. Marques F. Grand challenges in fuel cells: materials issues at all length scales. Front Energy Res. 2013;1:1–5.

9. Takahashi T, Iwahara H. Solid-state ionics—protonic conduction in perovskite type oxide solid solutions. Rev Chim Miner. 1980;17:243–53.

10. Iwahara H, Esaka T, Uchida H, Maeda N. Proton conduction in sintered oxides and its application to steam electrolysis for hydrogen-production. Solid State Ion. 1981;3–4:359–63.

11. Iwahara H, Uchida H, Ono K, Ogaki K. Proton conduction in sintered oxides based on $BaCeO_3$. J Electrochem Soc. 1988;135:529–33.

12. Bonanos N, Knight KS, Ellis B. Perovskite solid electrolytes—structure, transport-properties and fuel-cell applications. Solid State Ion. 1995;79:161–70. doi:10.1016/0167-2738(95)00056-C.

13. Norby T. Solid-state protonic conductors: principles, properties, progress and prospects. Solid State Ion. 1999;125:1–4. doi:10.1016/S0167-2738(99)00152-6.

14. Bohn HG, Schober T. Electrical conductivity of the high-temperature proton conductor $BaZr_{0.9}Y_{0.1}O_{2.95}$. J Am Ceram Soc. 2000;83:768–72. doi:10.1111/j.1151-2916.2000.tb01272.x.

15. Kreuer KD. Proton-conducting oxides. Annu Rev Mater Res. 2003;33:333–59. doi:10.1146/annurev.matsci.33.022802.091825.

16. Zhong Z. Stability and conductivity study of the $BaCe_{0.9-x}Zr_xY_{0.1}O_{2.95}$ systems. Solid State Ion. 2007;178:213–20. doi:10.1016/j.ssi.2006.12.007.

17. Madhavan B, Ashok A. Review of nanoperovskites: materials, synthesis and applications for proton and oxide ion conductivity. Ionics. 2015;21:601–10. doi:10.1007/s11581-014-1340-8.

18. Gonçalves MD, Maram PS, Navrotsky A, Muccillo R. Effect of synthesis atmosphere on the proton conductivity of Y-doped barium zirconate solid electrolytes. Ceram Int. 2016;42:13689–96. doi:10.1016/j.ceramint.2016.05.167.

19. Yamazaki Y, Hernandez-Sanchez R, Haile SM. Cation non-stoichiometry in yttrium-doped barium zirconate: phase behavior, microstructure, and proton conductivity. J Mater Chem. 2010;20:8158–66. doi:10.1039/C0JM02013C.

20. Cervera RB, Oyama Y, Yamaguchi S. Low temperature synthesis of nanocrystalline proton conducting $BaZr_{0.8}Y_{0.2}O_3$-δ by sol gel method. Solid State Ion. 2007;178:569–74. doi:10.1016/j.ssi.2007.01.010.

21. Khani Z, Taillades-Jacquin M, Taillades G, Marrony M, Jones DJ, Roziere J. New synthesis of nanopowders of proton conducting materials. A route to densified proton ceramics. J Solid State Chem. 2009;182:790–8. doi:10.1016/j.jssc.2008.12.020.

22. Antunes I, Brandao A, Figueiredo FM, Frade JR, Gracio J, Fagg DP. Mechanosynthesis of nanopowders of the proton-conducting electrolyte material Ba(Zr,Y)O3-δ. J Solid State Chem. 2009;182:2149–56. doi:10.1016/j.jssc.2009.05.027.

23. Duval SBC, Hostappels P, Vogt UF, Stimming U, Graule T. Characterization of $BaZr_{0.9}Y_{0.1}O_3$-δ prepared by three different synthesis methods: study of the sinterability and the conductivity. Fuel Cells. 2009;9:613–21. doi:10.1002/fuce.200800170.

24. Tong JH, Clark D, Bernau L, Sandres M, O'Hayre R. Solid-state reactive sintering mechanism for large-grained yttrium-doped barium zirconate proton conducting ceramics. J Mater Chem. 2010;20:6333–41. doi:10.1039/c0jm00381f.

25. Dahl PI, Lein HL, Yu YD, Tolchard J, Grande T, Eisnarsrud MA, Kiolseth C, Norby T, Haugsrud R. Microstructural characterization and electrical properties of spray pyrolyzed conventionally sintered or hot-pressed $BaZrO_3$ and $BaZr_{0.9}Y_{0.1}O_3$-δ. Solid State Ion. 2011;182:32–40. doi:10.1016/j.ssi.11.032.

26. Bi L, Traversa E. Synthesis strategies for improving the performance of doped-$BaZrO_3$ materials in solid oxide fuel cell applications. J Mater Res. 2014;29:1–15. doi:10.1557/jmr.2013.205.

27. Lavand AB, Malghe YS. Synthesis of nanosized $BaZrO_3$ from oxalate precursor. J Therm Anal Calorim. 2014;118:1613–8. doi:10.1007/s10973-014-403307.

28. Gonçalves MD, Maram PS, Muccillo R, Navrotsky A. Enthalpy of formation and thermodynamic insights into yttrium doped $BaZrO_3$. J Mater Chem A. 2014;2:17840–7. doi:10.1039/C4TA03487B.

29. Park KY, Seo Y, Kim KB, Song SJ, Park B, Park JY. Enhanced proton conductivity of yttrium-doped barium zirconate with sinterability in protonic ceramic fuel cells. J Alloys Compd. 2015;639:435–44. doi:10.1016/j.jallcom.2015.03.168.

30. Biswas M, An H, Choi SM, Son J-W, Lee J-H, Kim B-K, Lee H-W, Yoon KJ. Low temperature sintering of Ba(Zr,Y)O3-based proton conducting oxides using BaO–CuO eutectic flux as sintering aid. Ceram Int. 2016;42:10476–81. doi:10.1016/j.ceramint.2016.03.038.

31. Bozza F, Bator K, Kubiak WW, Graule T. Effects of Ni doping on the sintering and electrical properties of $BaZr_{0.8}Y_{0.2}O_3$-δ proton conducting electrolyte prepared by flame spray synthesis. J Eur Ceram Soc. 2016;36:101–7. doi:10.1016/j.jeurceramsoc.2015.09.010.

32. Shafi SP, Bi L, Boulfrad S, Traversa E. Y and Ni co-doped $BaZrO_3$ as a proton-conducting solid oxide fuel cell electrolyte exhibiting superior power performance. J Electrochem Soc. 2015;162:F1498–503. doi:10.1149/2.0701514jes.

33. Gazda M, Mielewczyk-Gryn A, Gdula-Kasica K, Wachowski S. Proton conducting ceramic powder synthesis by a low temperature method. J Nanosci Nanotechnol. 2015;15:3626–35. doi:10.1166/jnn.2015.9858.

34. Gao DY, Guo RS. Densification and properties of barium zirconate ceramics by addition of P_2O_5. Mater Lett. 2010;64:573–5. doi:10.1016/j.matlet.2009.12.003.

35. Chen C-T, Danel CE, Kim S. On the origin of the blocking effect of grain boundaries on proton transport in yttrium-doped barium zirconates. J Mater Chem. 2011;21:5435–42. doi:10.1039/C0JM03353G.

36. Babilo P, Haile SM. Enhanced sintering of yttrium-doped barium zirconate by addition of ZnO. J Am Ceram Soc. 2005;88:2362–8. doi:10.1111/j.1551-2916.2005.00449.x.

37. Tao SW, Irvine JTS. A stable, easily sintered proton-conducting oxide electrolyte for moderate-temperature fuel cells and electrolyzers. Adv Mater. 2006;18:1581–4. doi:10.1002/adma.200502098.

38. Tao SW, Irvine JTS. Conductivity studies of dense yttrium-doped $BaZrO_3$ sintered at 1325°C. J Solid State Chem. 2007;180:3493–503. doi:10.1016/j.jssc.2007.09.27.

39. Wang H, Peng R, Wu X, Hu J, Xia C. Sintering behavior and conductivity study of yttrium-doped BaCeO$_3$–BaZrO$_3$ solid solutions using ZnO additives. J Am Ceram Soc. 2009;92:2623–9. doi:10.1111/j.1551-2916.2009.03204.x.

40. Aleksandrovskii VV, Venskovskii NU, Kaleva GM, Politova ED, Prutchenko SG, Rudnitskii LA, Stefanovich SY, Khortova AY. Phase composition, microstructure, and thermal expansion of B$_2$O$_3$-modified LaGaO$_3$-based ceramics. Inorg Mater. 2001;37:641–6. doi:10.1023/A:1017580703909.

41. Hasegawa Y, Tamura S, Imanaka N. Effect of low-melting oxide additives on the sinterability and ion conductivity of Al^{3+} ion conducting solid electrolytes with the NASICON type structure. J New Mater Electrochem Syst. 2005;8:203–7.

42. Kishimoto H, Sakai N, Yamagi K, Horita T, Xiong Y-P, Brito ME, Yokokawa H. Destabilization of cubic-stabilized zirconia electrolyte induced by boron oxide under reducing atmosphere. J Mater Sci. 2009;44:639–46. doi:10.1007/s10853-008-3061-8.

43. Pasierb P, Gajerski R, Osiadly M, Lacz A. Application of DTA–TG–MS for determination of chemical stability of BaCeO$_3$-δ-based protonic conductors. J Therm Anal Calorim. 2014;117:683–91.

44. Oliveira IR, Studart AR, Innocentini MDM, Nascimento LA, Pandolfelli VC. Influence of dispersants in Al$_2$O and Al$_2$O$_3$–MgO refractory castables. Cerâmica. 2004;50:1–6.

45. Kleitz M, Kennedy JH. Resolution of multicomponent impedance diagrams. In: Vashishta P, Mundy JN, Shenoy GK, editors. Fast ion transport in solids. Amsterdam: Elsevier North Holland; 1979. p. 185–8.

46. Barsoukov E, Macdonald JR. Impedance spectroscopy: theory, experiment, and applications. London: Wiley; 2005. ISBN-13: 978-0471647492.

47. Hiraiva C, Han DL, Kuramitsu A, Kuwabara A, Takeuchi H, Majima M, Uda T. Chemical expansion and change in lattice constant of Y-doped BaZrO$_3$ by hydration/dehydration reaction and final heat-treating temperature. J Am Ceram Soc. 2013;96:879–84. doi:10.1111/jace.12172.

48. Earnest CM. Calorimetric heat of transition assignments by microcomputer-based differential thermal analysis: part II. The γ–β (orthorhombic to hexagonal) transition of barium carbonate. Thermochim Acta. 1989;137:365–71. doi:10.1016/0040-6031(89)87228-4.